



Cite this: DOI: 10.1039/c4ob01270d

A design strategy for small molecule-based targeted MRI contrast agents: their application for detection of atherosclerotic plaques†

Shimpei Iwaki,^a Kazuya Hokamura,^b Mikako Ogawa,^c Yasuo Takehara,^d Yasuaki Muramatsu,^a Takehiro Yamane,^a Kazuhisa Hirabayashi,^a Yuji Morimoto,^e Kohsuke Hagsawa,^f Kazuhide Nakahara,^g Tomoko Mineno,^g Takuya Terai,^a Toru Komatsu,^{a,h} Tasuku Ueno,^a Keita Tamura,ⁱ Yusuke Adachi,ⁱ Yasunobu Hirata,^j Makoto Arita,^a Hiroyuki Arai,^a Kazuo Umemura,^b Tetsuo Nagano^k and Kenjiro Hanaoka^{*a}

Gadolinium(III) ion (Gd^{3+}) complexes are widely used as contrast agents in magnetic resonance imaging (MRI), and many attempts have been made to couple them to sensor moieties in order to visualize biological phenomena of interest inside the body. However, the low sensitivity of MRI has made it difficult to develop practical MRI contrast agents for *in vivo* imaging. We hypothesized that practical MRI contrast agents could be designed by targeting a specific biological environment, rather than a specific protein such as a receptor. To test this idea, we designed and synthesized a Gd^{3+} -based MRI contrast agent, **2BDP3Gd**, for visualizing atherosclerotic plaques by linking the Gd^{3+} -complex to the lipophilic fluorophore BODIPY to stain lipid-rich environments. We found that **2BDP3Gd** was selectively accumulated into lipid droplets of adipocytes at the cellular level. Atherosclerotic plaques in the aorta of Watanabe heritable hyperlipidemic (WHHL) rabbits were clearly visualized in T_1 -weighted MR images after intravenous injection of **2BDP3Gd** *in vivo*.

Received 19th June 2014,
Accepted 13th August 2014
DOI: 10.1039/c4ob01270d

www.rsc.org/obc

Introduction

Magnetic resonance imaging (MRI) is widely used for noninvasive imaging in both clinical medicine and life sciences. MR images are constructed from 1H NMR signals mainly derived from water protons, so the signal intensity depends upon the concentration and relaxation times (T_1 and T_2) of water molecules. Paramagnetic ions such as the gadolinium(III) ion (Gd^{3+}) effectively shorten the T_1 (spin-lattice) relaxation time of water protons by promoting rapid exchange of inner-sphere water molecules with bulk water, and enhance the signal intensity in T_1 -weighted MR images. Gd^{3+} complexes are widely used as MRI contrast agents to enhance tissue contrast inside the body.¹

Compared with other imaging modalities such as fluorescence imaging, ultrasound and PET, MRI provides high spatial resolution deep within tissues.² Therefore, its application for *in vivo* imaging is important, and many Gd^{3+} complex-based MRI contrast agents have been developed for this purpose.^{1,3} In general, there are two design strategies for functional MRI contrast agents. One is to employ “smart” MRI contrast agents that induce a change of the water proton relaxation time (T_1 or T_2) when they are structurally modified by

^aGraduate School of Pharmaceutical Sciences, The University of Tokyo, 7-3-1 Hongo, Bunkyo-ku, Tokyo 113-0033, Japan. E-mail: khanaoka@mol.f.u-tokyo.ac.jp; Fax: +81 3 5841 4855; Tel: +81 3 5841 4852

^bDepartment of Pharmacology, Hamamatsu University School of Medicine, 1-20-1 Handayama, Hamamatsu, Shizuoka 431-3192, Japan

^cPhoton Medical Research Center, Hamamatsu University School of Medicine, 1-20-1 Handayama, Hamamatsu, Shizuoka 431-3192, Japan

^dDepartment of Radiology, Hamamatsu University School of Medicine, 1-20-1 Handayama, Hamamatsu, Shizuoka 431-3192, Japan

^eDepartment of Integrative Physiology and Bio-Nano Medicine, National Defense Medical College, Namiki 3-2, Tokorozawa, Saitama 359-8513, Japan

^fDepartment of Physiology, National Defense Medical College, Namiki 3-2, Tokorozawa, Saitama 359-8513, Japan

^gFaculty of Pharmacy, Takasaki University of Health and Welfare, 60 Nakaorui, Takasaki-shi, Gunma 370-0033, Japan

^hJST, PRESTO, 5 Sanbancho, Chiyoda-ku, Tokyo 102-0075, Japan

ⁱDepartment of Physiology, Graduate School of Medicine, The University of Tokyo, 7-3-1 Hongo, Bunkyo-ku, Tokyo 113-0033, Japan

^jDepartment of Cardiovascular Medicine, Graduate School of Medicine, The University of Tokyo, 7-3-1 Hongo, Bunkyo-ku, Tokyo 113-0033, Japan

^kOpen Innovation Center for Drug Discovery, The University of Tokyo, 7-3-1 Hongo, Bunkyo-ku, Tokyo 113-0033, Japan

† Electronic supplementary information (ESI) available: Supplementary methods, figures, tables and video. See DOI: 10.1039/c4ob01270d

exposure to a target, such as a specific enzyme activity.^{4–6} The other is to conjugate Gd^{3+} complexes to specific ligands or antibodies directed to the targeted biomolecules.^{5,7,8} However, there are few examples of application of functional MRI contrast agents based on the former strategy for *in vivo* whole-body imaging because it is very difficult to control the bio-distribution within the body. In the case of the latter strategy, the low sensitivity of the MRI technique makes it difficult to develop practical MRI contrast agents for *in vivo* imaging.³ In general, the detection limit of the Gd^{3+} complex in MRI measurements is around several μM ,⁹ whereas target biomolecules are often present only at the nanomolar order of concentration.^{10,11} To achieve sensitive detection, a new strategy to achieve sufficient accumulation of MRI contrast agents in the target region is required. Toward this end, we hypothesized that MRI contrast agents targeted to specific biological environments of interest, rather than to specific proteins such as receptors, could be efficiently accumulated in the target region at a sufficient concentration to allow clear MRI-based visualization of biological phenomena, irrespective of the concentrations of specific target biomolecules.

To validate this concept, we tried to develop MRI contrast agents for atherosclerosis. Atherosclerosis is a progressive disease characterized by accumulation of lipids and fibrous elements in the form of atherosclerotic plaques in large arteries.¹² Its most important clinical complication is acute occlusion due to the formation of a thrombus or blood clot, which is usually associated with plaque rupture, and results in myocardial infarction or stroke.^{13,14} Atherosclerosis is a primary cause of heart disease and stroke, and is the underlying cause of about 30% of all deaths in westernized societies.¹⁵ Therefore, the detection of atherosclerotic plaques is very important both in clinical medicine and life science. To develop suitable MRI contrast agents, we focused on staining dyes for atherosclerotic plaques. Sudan IV and Oil red O are widely used in histology for staining not only lipid droplets, which are lipid storage compartments surrounded by a phospholipid monolayer, in adipocytes,¹⁶ but also the lipid cores of

atherosclerotic plaques.^{17,18} So, we anticipated that the gadolinium ion complex conjugated with these dyes would accumulate in the lipid cores of atherosclerotic plaques, irrespective of the concentrations of specific target biomolecules. However, general protocols for staining with Sudan IV and Oil red O include incubation with organic solvents such as isopropanol,¹⁹ so that these scaffolds would not be suitable for *in vivo* imaging. Instead, we focused on the lipophilic fluorophore BODIPY (boron dipyrromethene) as a candidate atherosclerotic targeting moiety, since BODIPY is also used for staining lipid droplets in adipocytes, but does not require incubation in an organic solvent.^{16,19} Thus, we expected that the BODIPY- Gd^{3+} complex conjugate would be accumulated in atherosclerotic plaques *in vivo*.

Results

Molecular design of MRI contrast agents for atherosclerotic plaques

To validate the concept, we designed and synthesized a Gd^{3+} complex conjugated with a BODIPY moiety, **BDP-Gd**,²⁰ as a MRI contrast agent candidate for atherosclerotic plaques (Fig. 1a). BODIPY is a widely used fluorophore which has a high extinction coefficient (ϵ) and a high quantum yield of fluorescence (Φ_{fl}).²¹ An additional advantage of BODIPY is that the contrast agent would be detectable not only by MRI, but also by fluorescence measurements, because the BODIPY moiety is a fluorophore. With such MRI-fluorescence dual-modal probes,^{22,23} the contrast agent distribution inside cells or tissues can be precisely evaluated by means of fluorescence microscopy observation.

Fluorescence imaging of contrast agent distribution in live cells

First, we applied **BDP-Gd** to live adipocytes and observed its intracellular localization with a fluorescence microscope (Fig. 1b). Strong fluorescence of the BODIPY moiety was observed selectively in lipid droplets in adipocytes, but not in preadipocytes, as

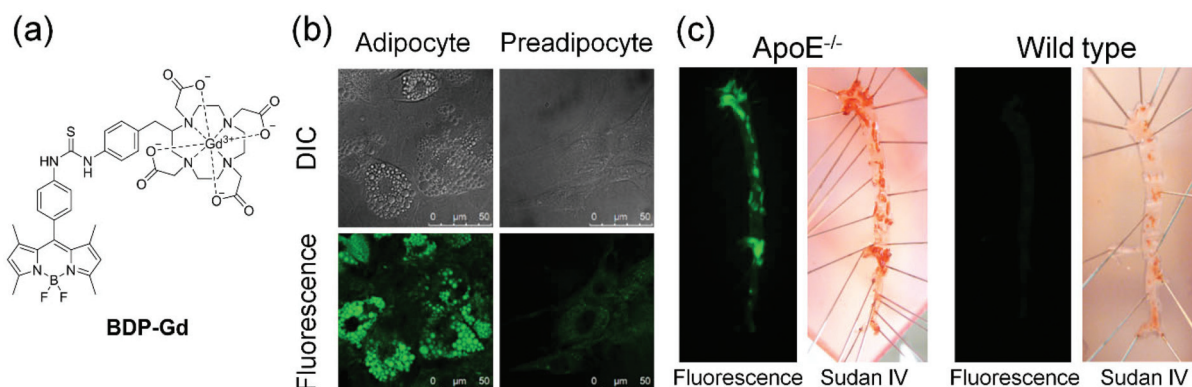


Fig. 1 (a) Chemical structure of **BDP-Gd**. (b) Confocal microscopy images of adipocytes (left) and preadipocytes (right) loaded with **BDP-Gd** ($10 \mu\text{M}$ in DMEM containing 0.1% DMSO as a cosolvent). Upper and lower panels show DIC and fluorescence images, respectively. (c) Fluorescence (left) and Sudan IV staining (right) images of the aorta isolated from *ApoE*^{-/-} or wild-type mice injected with **BDP-Gd** (1st injection; 5 mM, $100 \mu\text{L}$. 2nd injection; 5 mM, $150 \mu\text{L}$, 2 h after 1st injection). Fluorescence images were captured 1 h after the 2nd injection.

expected (Fig. 1b). This result indicates that **BDP-Gd** is indeed selectively accumulated in lipid-rich environments such as lipid droplets inside live cells.

Ex vivo fluorescence imaging of aorta of *ApoE*^{-/-} mice

We expected that **BDP-Gd** would also be accumulated in atherosclerotic plaques *in vivo*. To test this idea, we first performed fluorescence imaging of atherosclerotic plaques of *ApoE*^{-/-} mice, which are widely used mouse models of hyperlipidemia and atherosclerosis.¹⁷ Apolipoprotein E (ApoE) is the major component of lipoprotein and facilitates hepatic uptake of lipoproteins.¹⁷ Anesthetized mice were injected with **BDP-Gd** into the orbital vein and sacrificed 3 h later. Strong fluorescence of the BODIPY moiety was observed from atherosclerotic plaques in the isolated aorta of *ApoE*^{-/-} mice, and was colocalized with Sudan IV staining, while no marked fluorescence was seen in the case of wild-type mice (Fig. 1c). Sudan IV staining is often used to identify atherosclerotic plaques, so this result indicates that **BDP-Gd** accumulates preferentially in atherosclerotic plaques of *ApoE*^{-/-} mice.

Derivatization of BDP-Gd for *in vivo* application

Next, we applied **BDP-Gd** to MR imaging of atherosclerotic plaques of Watanabe heritable hyperlipidemic (WHHL) rabbits. The WHHL rabbit is an animal model of atherosclerosis caused by deficiency of the low density lipoprotein (LDL) receptor and is considered to be a better animal model of human atherosclerosis than *ApoE*^{-/-} mice because WHHL rabbits have similar lipoprotein metabolism to humans.²⁴ However, no clear increment of MR signal in atherosclerotic plaques was seen in WHHL rabbits injected with **BDP-Gd** (data not shown). The reasons for this may be that the sensitivity of **BDP-Gd** was insufficient and also that **BDP-Gd** was rapidly cleared from the body. Therefore, we next derivatized **BDP-Gd** in order to obtain a more sensitive MRI contrast agent.

First, to identify the essential chemical structure for accumulation in a lipid-rich environment, **BDP-DO3A-Gd**, **BDP-thio-DO3A-Gd**, **BDP-thioPh-DO3A-Gd**, **BDP-thio-BnDOTA-Gd** and **BDP-thioPh-BnDOTA-Gd** were designed and synthesized (Fig. 2). Adipocytes were loaded with these contrast agents, and the localization of the contrast agents inside the cells was observed under a fluorescence microscope. Only some of these contrast agents were specifically localized to lipid droplets of adipocytes, and it appeared that a common BODIPY-thiourea-phenyl structure is important for accumulation in lipid droplets. Furthermore, in order to obtain a sufficient Gd³⁺ concentration for MR imaging at the targeted region, we selected the reported multi (three) Gd³⁺ complex-bearing scaffold, which can show very high *r*₁ relaxivity,²⁵ as a backbone, and designed and synthesized contrast agents containing two (**2BDP3Gd**), one (**1BDP3Gd**) or no (**0BDP3Gd**) BODIPY-thiourea-phenyl moieties on this backbone as MRI contrast agent candidates (Fig. 3). Their relaxivities and photophysical properties are summarized in Table 1. **2BDP3Gd** and **1BDP3Gd** showed three to four times higher *r*₁ relaxivity per Gd³⁺ than a widely used MRI contrast agent, Magnevist® (Gd-

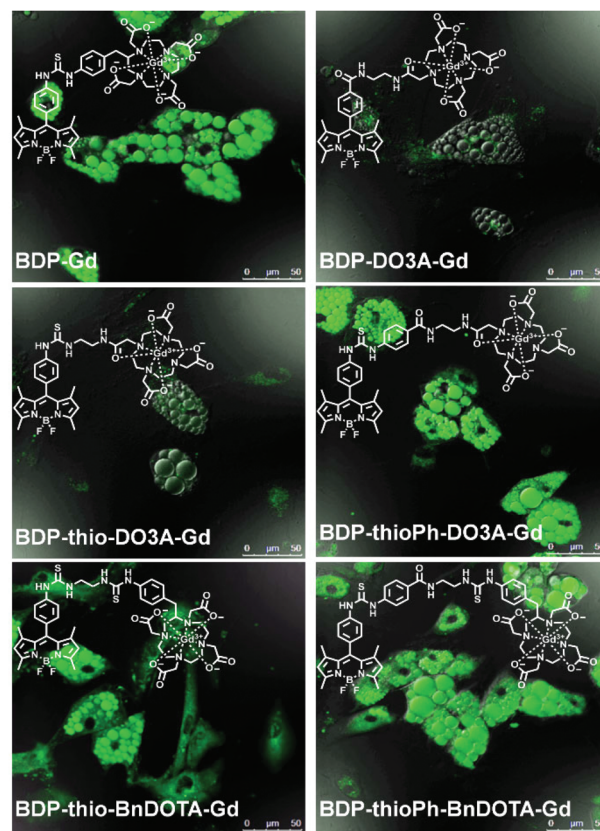


Fig. 2 Fluorescence images of adipocytes loaded with BDP-Gd derivatives. Confocal microscopy images of adipocytes loaded with BDP-Gd derivatives (10 μM in DMEM containing 0.1% DMSO as a cosolvent). (Top left) **BDP-Gd**, (top right) **BDP-DO3A-Gd**, (middle left) **BDP-thio-DO3A-Gd**, (middle right) **BDP-thioPh-DO3A-Gd**, (bottom left) **BDP-thio-BnDOTA-Gd**, (bottom right) **BDP-thioPh-BnDOTA-Gd**.

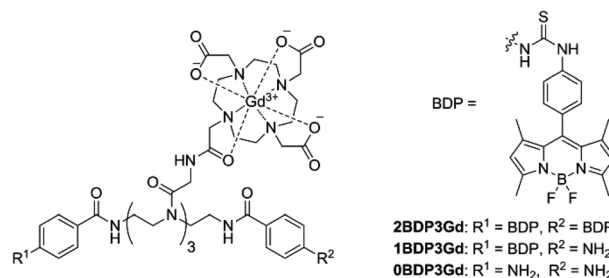


Fig. 3 Chemical structures of MRI contrast agents for atherosclerotic plaques.

Table 1 *r*₁ Relaxivity and photophysical properties

Probe	<i>r</i> ₁ ^a (mM ⁻¹ s ⁻¹)	λ _{abs} ^b (nm)	λ _{em} ^b (nm)	Φ _{fl} ^{b,c}
BDP-Gd	22	497	509	0.160
2BDP3Gd	50	507	512	0.010
1BDP3Gd	42	499	509	0.110
0BDP3Gd	31	—	—	—

^a All data were measured at 37 °C, 20 MHz in PBS. *r*₁ Relaxivity was calculated per molecule. ^b All data were measured in 100 mM HEPES buffer (pH 7.4). ^c Φ_{fl} is the relative fluorescence quantum yield determined using fluorescein in 0.1 M NaOH aq. (0.85) as a fluorescence standard.

DTPA; gadolinium(III) diethylenetriamine-*N,N,N',N',N''*-pentaacetic acid; the r_1 relaxivity of Magnevist® is $4.3 \text{ mM}^{-1} \text{ s}^{-1}$ in water (25 °C, pH 7.4)).¹ These high relaxivities may be due to the high hydrophobicity of BODIPY, *i.e.* **2BDP3Gd** and **1BDP3Gd** appear to show intermolecular stacking in aqueous solution, as judged from their low fluorescence quantum yields and their absorption spectra, and the resulting increment of the apparent molecular weight may lead to enhancement of the r_1 relaxivity due to slower molecular rotation of the Gd^{3+} complex.^{1,26} On the other hand, in organic solvents such as MeOH, **2BDP3Gd** and **1BDP3Gd** showed strong fluorescence without fluorescence quenching due to intermolecular stacking (Fig. S1 and Table S1, ESI†). When solutions of **2BDP3Gd**, **1BDP3Gd**, **0BDP3Gd** and Magnevist® were each dialyzed (MWCO: 25 000) for 24 h and the concentrations of Gd^{3+} complexes were determined by ICP-AES, we found that **2BDP3Gd** and **1BDP3Gd** were highly retained inside the dialysis membranes compared to **0BDP3Gd** and Magnevist® (Fig. S2, ESI†). This result supports the idea that **2BDP3Gd** and **1BDP3Gd** exhibit intermolecular stacking in aqueous solution because of their hydrophobic BODIPY moiety. The r_1 relaxivity values are also higher than would be expected for monomeric complexes such as Magnevist®, and the increment of the apparent molecular weight due to intermolecular stacking may contribute to this effect.²⁷

We examined **2BDP3Gd** and **1BDP3Gd** in cellular experiments, as well as **BDP-Gd**. These contrast agents were efficiently accumulated into lipid droplets of adipocytes (Fig. S3, ESI†). Furthermore, like **BDP-Gd**, they were accumulated in

atherosclerotic plaques of *ApoE*^{-/-} mice in *ex vivo* fluorescence imaging of the aorta (Fig. S4, ESI†). These results confirmed that we had successfully developed more sensitive MRI contrast agents that retained the ability to accumulate in lipid-rich environments at both the cellular level and intact mouse level.

In vivo MR imaging of atherosclerotic plaques of WHHL rabbits

Finally, we applied our improved MRI contrast agents to *in vivo* MR imaging of atherosclerotic plaques in WHHL rabbits. WHHL or wild-type rabbits were anesthetized, and T_1 -weighted MR images were obtained before contrast agent injection. Then, the rabbits were injected with **2BDP3Gd**, **1BDP3Gd** or **0BDP3Gd** into an ear vein, and T_1 -weighted MR images were obtained at 1, 2 and 24 h after the injection (Fig. 4). The MR signal intensity in the arterial wall of WHHL rabbits, but not wild-type rabbits, increased time-dependently when **2BDP3Gd** was injected, while no significant increment of MR signal in the arterial wall was seen in WHHL or wild-type rabbits injected with **0BDP3Gd** or **1BDP3Gd** (Fig. 4a and c). After the MR imaging, the rabbits were euthanized and the whole aorta was removed together with vertebrae for *ex vivo* MR imaging (Fig. 4b and d). When rabbits were injected with **2BDP3Gd**, the signal intensity of the isolated aorta of WHHL rabbits was higher than that of wild-type rabbits, while no clear difference was seen when **1BDP3Gd** was injected. Furthermore, in the fluorescence imaging of isolated aortas of rabbits, the strongest fluorescence was observed from the aorta of WHHL rabbits injected with **2BDP3Gd** (Fig. S5, ESI†).

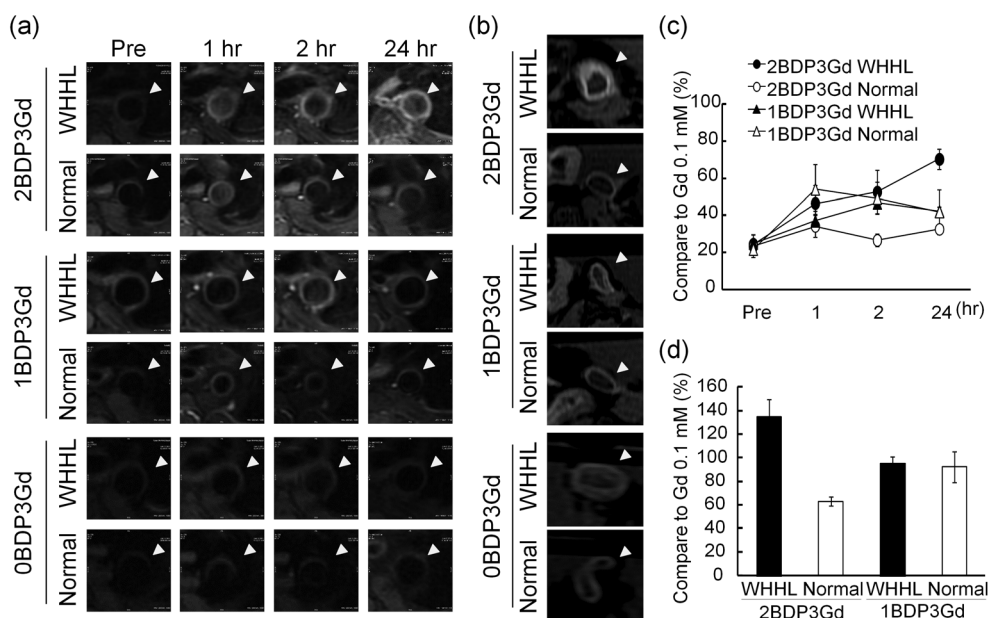


Fig. 4 (a) T_1 -Weighted MR images (*in vivo* imaging) of WHHL (upper) or normal (lower) rabbits before and after administration of **2BDP3Gd**, **1BDP3Gd** or **0BDP3Gd** ($7.4 \mu\text{mol kg}^{-1}$). White arrowheads indicate the aorta. (b) T_1 -Weighted MR images (*ex vivo* imaging) of the isolated aorta of WHHL (upper) or normal (lower) rabbits. White arrowheads indicate the aorta. (c) Time-dependent changes of the normalized MR signal intensity of the aorta in *in vivo* MR imaging of atherosclerotic plaques. The signal intensity was normalized by the MR signal intensity of a Gd^{3+} phantom (0.1 mM Magnevist®). Error bars show the standard deviation (3 ROIs). (d) MR signal intensity in *ex vivo* MR images of the isolated aorta. The signal intensity was normalized by the MR signal intensity of a Gd^{3+} phantom (0.1 mM Magnevist®). Error bars show the standard deviation (3 ROIs).

Histological staining of atherosclerotic plaques of WHHL rabbits

To confirm that **2BDP3Gd** was accumulated in atherosclerotic plaques, the aorta isolated from WHHL rabbits was histologically stained (Fig. 5). As shown by HE staining (Fig. 5e), thickening of the aorta and infiltration of leucocytes were observed, and the accumulation of lipids was also observed by means of Oil red O staining (Fig. 5b). Furthermore, the accumulation of fibrous elements was observed in the azan-stained image (Fig. 5d). These results indicate the presence of atherosclerotic plaques in the sample. The localization of the BODIPY fluorescence (Fig. 5a; green) was well matched with that of Oil red O staining (Fig. 5b), so the increment of the signal intensity in the arterial wall of WHHL rabbits appeared to be due to the accumulation of **2BDP3Gd** in the lipid-rich environment, such as lipid droplets, of atherosclerotic plaques. Interestingly, the BODIPY fluorescence was also well colocalized with α -actin staining (Fig. 5c), but not with the immunostaining of macrophages (Fig. 5a; red). This result indicates that **2BDP3Gd** accumulated mainly in foam cells derived from smooth muscle cells; indeed, many foam cells in atherosclerotic plaques of WHHL rabbits have been reported to be derived from smooth muscle cells.²⁸ Although the majority of foam cells in human atherosclerotic plaques are

thought to be derived from macrophages, foam cells derived from smooth muscle cells are also seen in human atherosclerotic plaques,²⁹ so we expected that **2BDP3Gd** would also be potentially useful for diagnosis of atherosclerosis in humans. On the other hand, only weak fluorescence of BODIPY was observed from the aorta of WHHL rabbits injected with **1BDP3Gd** (Fig. S6, ESI[†]), probably because a single BODIPY-thiourea-phenyl moiety is not enough to support sufficient accumulation of the contrast agent in atherosclerotic plaques for MR imaging. The reproducibility of the MR imaging of atherosclerotic plaques with **2BDP3Gd** and histological staining was confirmed using another WHHL rabbit (Fig. S7 and S8, ESI[†]). Thus, our strategy to target a lipid-rich environment for visualizing atherosclerotic plaques was proved to work at a practical level.

In vivo fluorescence imaging of atherosclerotic plaques of LDL receptor-deficient mice

2BDP3Gd is a lipophilic Gd³⁺ complex, so it is expected that **2BDP3Gd** would also accumulate in the adipose tissue or liver,^{20,30,31} as well as atherosclerotic plaques. However, atherosclerotic plaques are formed in the intima of arterial walls, so it should be straightforward to distinguish MRI signal changes in atherosclerotic plaques from those in adipose tissues or liver. Indeed, we successfully visualized atherosclerotic plaques of WHHL rabbits by MRI as shown in Fig. 4. To support this, we carried out *in vivo* fluorescence imaging of atherosclerotic plaques of LDL receptor-deficient mice.³² **2BDP3Gd** was intravenously injected, and fluorescence imaging of the carotid artery of LDL receptor-deficient mice was performed *in vivo* (Fig. S9, ESI[†]). The plaque to fatty tissue ratio of the fluorescence signal intensity did not exceed 1, whereas the plaque to carotid artery ratio was in the range of 1.5 to 15. It is important to note that specificity against the normal arterial wall is the critical issue, not that against the liver or fatty tissue. Indeed, although strong fluorescence of **2BDP3Gd** was observed from adipose tissue, we successfully identified atherosclerotic plaques in the carotid artery *in vivo*. Furthermore, we could also identify atherosclerotic plaques in the aorta by fluorescence endoscopy in real-time *in vivo* (Fig. S10 and video S1, ESI[†]). These data indicate that accumulation of **2BDP3Gd** in adipose tissue does not impair visualization of atherosclerotic plaques.

Discussion

Because MRI can provide high-spatial-resolution images of sites deep inside tissues, it is suitable for imaging of atherosclerosis.³³ Some MRI contrast agents for atherosclerosis have been reported,^{34,35} and most of them are Gd³⁺ complexes or magnetic nanoparticles conjugated to specific ligands or antibodies that are directed towards atherosclerotic markers such as adhesion molecules (VCAM-1,³⁶ integrin $\alpha_v\beta_3$ ³⁷ and selectin^{38,39}), a scavenger receptor of macrophages⁴⁰ and fibrin.^{41,42} Furthermore, to obtain higher sensitivity, liposomes,⁴³ nano-

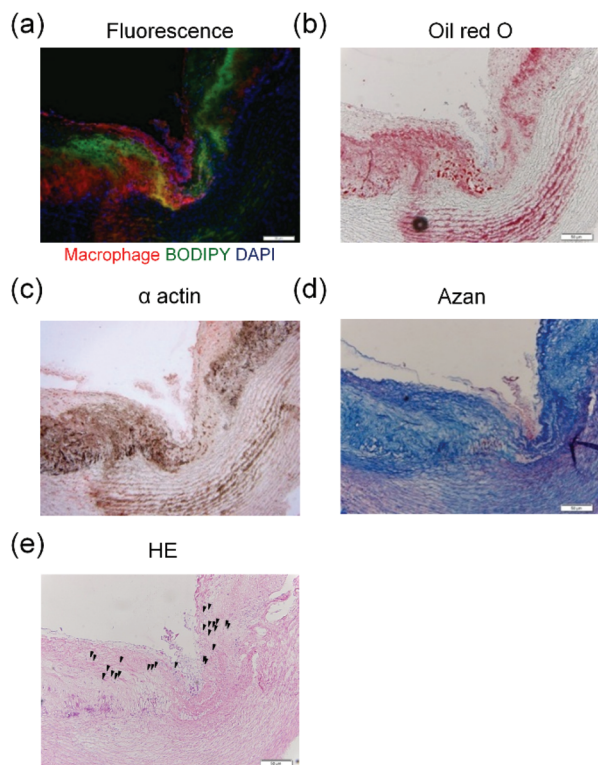


Fig. 5 Frozen section of the aorta of WHHL rabbits after administration of **2BDP3Gd**. Frozen sections were histologically examined by (a) fluorescence imaging (red: anti-RAM antibody, green: **2BDP3Gd**, blue: DAPI), (b) Oil red O staining, (c) α -actin (smooth muscle cell marker) staining, (d) azan staining, and (e) haematoxylin and eosin (HE) staining. Black arrowheads in (e) indicate leucocytes. Scale bar: 50 μ m.

particles⁴⁴ and micelles^{40,45} containing 10^3 – 10^4 Gd^{3+} and targeting moieties have been developed. However, the target biomolecules for atherosclerosis are present in plaques only at the nanomolar concentration.³³ On the other hand, our alternative strategy to target a specific environment enables efficient accumulation of the MRI contrast agent in atherosclerotic plaques, irrespective of the concentrations of specific target biomolecules. Therefore, in principle, **2BDP3Gd** should be effective for the sensitive detection of atherosclerotic plaques. Very recently, an elastic layer-specific MRI contrast agent based on a similar design strategy was reported,³⁴ and this contrast agent could also successfully visualize atherosclerotic plaques. However, although this elastic layer-specific MRI contrast agent can evaluate the morphology of arterial walls, our contrast agent can visualize atherosclerotic plaques with large lipid cores, which tend to rupture easily.⁴² Thus, our contrast agent should be more suitable to predict risk. In addition, an MR angiography experiment showed that **2BDP3Gd** has a longer half-life in the circulation than **0BDP3Gd** (Fig. S11, ESI†). It is known that lipophilic Gd^{3+} complexes bind to serum albumin,^{1,46,47} and albumin binding prevents the Gd^{3+} complexes from being excreted through the kidneys and extends their circulation time.⁴⁶ Indeed, the binding of **2BDP3Gd** to serum albumin was confirmed by *in vitro* fluorescence measurement (Fig. S12 and S13, ESI†). **2BDP3Gd** also binds to LDL *in vitro* and *in cellulo* (Fig. S12–S14, ESI†). The binding of **2BDP3Gd** to serum albumin or LDL may contribute to the long-circulation property of **2BDP3Gd**. The fortuitously prolonged circulation time of **2BDP3Gd** may also contribute to its efficient accumulation into atherosclerotic plaques.⁴⁸ We also examined the toxicity of **2BDP3Gd** after i.v. injection into JCl:ICR mice ($n = 5$) at the same dose as used in the MRI experiment ($7.4 \mu\text{mol kg}^{-1}$). No mice died within 10 days, and thus **2BDP3Gd** did not show serious acute toxicity at the dose used, although we cannot rule out the risk of nephrogenic systemic fibrosis (NSF), a rare but serious side effect of Gd^{3+} contrast agents.^{23,49}

Conclusions

We have developed a new design strategy focusing on a lipid-rich environment in order to visualize atherosclerotic plaques by means of MRI. Among the contrast agent candidates examined, the lipophilic BODIPY-thiourea-phenyl moiety was identified as an essential structure for recognition of lipid-rich environments, such as lipid droplets of atherosclerotic plaques, *in vitro*. We established that **2BDP3Gd** containing this structure was accumulated preferentially in atherosclerotic plaques in the *ApoE*^{-/-} mouse model of atherosclerosis. **2BDP3Gd** was also able to visualize atherosclerotic plaques in the aorta of WHHL rabbits in T_1 -weighted MR images *in vivo*. Moreover, the BODIPY moiety enabled precise observation of the localization of **2BDP3Gd** inside the artery *ex vivo* by means of fluorescence microscopy, providing the capability for multimodal imaging. *In vivo* fluorescence imaging of atherosclerotic

plaques of LDL receptor-deficient mice was also performed by the use of an endoscope, showing that this agent enables real-time visualization of atherosclerotic plaques *in vivo*. Thus, our environment-targeting design strategy is effective for the molecular design of practical MRI contrast agents for *in vivo* whole-body imaging of lipid-rich environments such as atherosclerotic plaques. It should also be possible to extend this design strategy to other pathological environments, such as hypoxia^{50,51} and the relatively low pH environment of tumors.^{52,53}

Methods

Supplementary methods

Experimental details of general procedures, materials, instruments, synthesis, fluorometric analysis, relaxivity measurements, cell culture, fluorescence microscopic imaging of adipocytes, *in vivo* fluorescence imaging of LDLR^{-/-} mice and ultrathin endoscopic fluorescence imaging can be found in the ESI.†

Ex vivo imaging of mouse aorta

Mice were fixed on a custom-made cradle and anesthetized continuously with a mixture of oxygen and isoflurane (1.5–2.0%). Then, 5 mM probe solution in saline (100 μL) was administered to the mouse *via* the orbital vein. An additional probe solution (150 μL) was administered to the same mouse *via* the orbital vein at 120 min after the first injection. The mouse was sacrificed by perfusion fixation with 4% formaldehyde at 60 min after the second injection. The full-length aorta was carefully isolated and longitudinally opened. Fluorescence images of the aorta were captured with a MaestroTM In-Vivo Imaging System (Perkin Elmer). The excitation wavelength was 445–490 nm, and the fluorescence emission wavelength was 520–800 nm. Next, atherosclerotic plaques were visualized by Sudan IV staining, *i.e.* the aorta was fixed with 10% formalin solution for 30 min, and then washed with 70% EtOH for 3 min. After that, 0.5% (w/v) Sudan IV staining solution (in acetone–70% EtOH, 30% H₂O = 50/50) was added and the preparation was shaken for 15 min. To remove excess Sudan IV, the aorta was washed with 70% EtOH for 3 min and with water for 5 min. Then, bright-field images of the aorta were captured with a compact digital camera (FinePix F40fd, FUJIFILM).

MR imaging of atherosclerotic plaques of rabbits

Watanabe heritable hyperlipidemic (WHHL) rabbits and normal Japanese white (JW) rabbits were purchased from Kitayama Labes (Nagano, Japan). Animals under general anesthesia with continuous inhalation of oxygen containing isoflurane (2.0–2.5%) (Escaïne; Mylan Pharma Co., Tokyo, Japan) were subjected to MR imaging in the supine position with a superconducting MR scanner (Signa HDxt 3.0 T, GE Healthcare, WI, USA), using an 8-channel phased array knee coil. T_1 -Weighted images were acquired before and at 1 h, 2 h

and 24 h after intravenous injection of the probe solution in saline (5 mM, 7.4 $\mu\text{mol kg}^{-1}$) via the marginal pinna vein. The parameters used for the ECG gated double IR prepared fast spin echo sequence were median TR (ms)/ef TE (ms)/FA (degree) of 261/8.6/90, a matrix size of 320 \times 256; a FOV (cm) of 12 \times 9 for axial and 18 \times 18 for sagittal, a slice thickness (mm) of 3.0, an echo train of 2, section intervals (mm) of 5 for axial and 0 for sagittal, and the average number of signals (NEX) of 4.

For MR angiography, the coronal IR prepared 3-dimensional Fast Spoiled Gradient Echo sequence was used with the following parameters; TR (ms)/TE (ms)/FA (degree) of 4.3–4.7/1.4–1.6/15, a matrix size of 320 \times 160; a FOV (cm) of 17.8 \times 12.5, a slice thickness (mm) of 6 and the NEX of 1.

After the imaging, animals were euthanized and the whole aorta was removed with vertebrae for *ex vivo* MR imaging. In this case, the pulse sequence and the parameters used were axial conventional spin echo, TR (ms)/TE (ms) of 300/11, a matrix size of 384 \times 160; a FOV (cm) of 9 \times 6.8, a slice thickness (mm) of 1, section intervals (mm) of 2.5, and the NEX of 12. The average intensities of the vessel wall and the phantom (0.1 mM) were measured by placing three regions of interest (ROIs) on the vessel wall and the largest possible ROI on the phantom. Then, the three values for the vessel wall were averaged, and divided by the value for the phantom. Error bars show the standard deviation of the signal intensities of the three ROIs.

Fluorescence imaging of the isolated WHHL rabbit aorta

Fluorescence images of the aorta (ESI Fig. S4†) were captured with a Maestro™ 2 (Perkin Elmer). The excitation wavelength was 457 \pm 22.5 nm, and fluorescence emission (>490 nm) was observed.

Histological staining of the isolated WHHL rabbit aorta

Aortic sections were subjected to HE, Azan-Mallory or Oil red O staining. Immunohistochemistry was performed according to reported methods,⁵⁴ using anti-rabbit macrophage monoclonal antibody (RAM-11, Dako Corp., Santa Barbara, CA, USA)⁵⁵ or anti-alpha-actin monoclonal antibody (M0851, Dako Corp., Santa Barbara, CA, USA). The second antibody for macrophages was Fluoromount (goat anti mouse Alexa 594, Diagnostic BioSystems, USA).

Acknowledgements

This work was supported in part by MEXT (Specially Promoted Research Grant no. 22000006 to T.N., and Grants 24689003 and 24659042 to K.H.). K.H. was also supported by Grants-in-Aid from the Takeda Science Foundation, the Uehara Memorial Foundation, the Hattori Hokokai Foundation, the Inoue Foundation for Science, The Research Foundation for Pharmaceutical Sciences and the Astellas Foundation for Research on Metabolic Disorders. The authors thank Dr Michiaki Kumagai

at Kyushu University for helpful discussions. S.I. was supported by a Grant-in-Aid for JSPS Fellows.

Notes and references

- 1 P. Caravan, J. J. Ellison, T. J. McMurry and R. B. Lauffer, *Chem. Rev.*, 1999, **99**, 2293–2352.
- 2 R. Weissleder and M. J. Pittet, *Nature*, 2008, **452**, 580–589.
- 3 E. Terreno, D. D. Castelli, A. Viale and S. Aime, *Chem. Rev.*, 2010, **110**, 3019–3042.
- 4 A. Y. Louie, M. M. Hüber, E. T. Ahrens, U. Rothbächer, R. Moats, R. E. Jacobs, S. E. Fraser and T. J. Meade, *Nat. Biotechnol.*, 2000, **18**, 321–325.
- 5 J. L. Major and T. J. Meade, *Acc. Chem. Res.*, 2009, **42**, 893–903.
- 6 K. Hanaoka, *Chem. Pharm. Bull.*, 2010, **58**, 1283–1294.
- 7 L. Frullano, C. Wang, R. H. Miller and Y. Wang, *J. Am. Chem. Soc.*, 2011, **133**, 1611–1613.
- 8 L. M. De León-Rodríguez, A. Lubag, D. G. Udugamasooriya, B. Proneth, R. A. Brekken, X. Sun, T. Kodadek and A. Dean Sherry, *J. Am. Chem. Soc.*, 2010, **132**, 12829–12831.
- 9 K. Hanaoka, A. J. M. Lubag, A. Castillo-Muzquiz, T. Kodadek and A. D. Sherry, *Magn. Reson. Imaging*, 2008, **26**, 608–617.
- 10 G. J. Kelloff, K. A. Krohn, S. M. Larson, R. Weissleder, D. A. Mankoff, J. M. Hoffman, J. M. Link, K. Z. Guyton, W. C. Eckelman, H. I. Scher, J. O'Shaughnessy, B. D. Cheson, C. C. Sigman, J. L. Tatum, G. Q. Mills, D. C. Sullivan and J. Woodcock, *Clin. Cancer Res.*, 2005, **11**, 7967–7985.
- 11 W. S. El-Deiry, C. C. Sigman and G. J. Kelloff, *J. Clin. Oncol.*, 2006, **24**, 3261–3273.
- 12 A. J. Lusis, *Nature*, 2000, **407**, 233–241.
- 13 R. Ross, *N. Engl. J. Med.*, 1999, **340**, 115–126.
- 14 C. K. Glass and J. L. Witztum, *Cell*, 2001, **104**, 503–516.
- 15 V. L. Roger, A. S. Go, D. M. Lloyd-Jones, E. J. Benjamin, J. D. Berry, W. B. Borden, D. M. Bravata, S. Dai, E. S. Ford, C. S. Fox, H. J. Fullerton, C. Gillespie, S. M. Hailpern, J. A. Heit, V. J. Howard, B. M. Kissela, S. J. Kittner, D. T. Lackland, J. H. Lichtman, L. D. Lisabeth, D. M. Makuc, G. M. Marcus, A. Marelli, D. B. Matchar, C. S. Moy, D. Mozaffarian, M. E. Mussolino, G. Nichol, N. P. Paynter, E. Z. Soliman, P. D. Sorlie, N. Sotoodehnia, T. N. Turan, S. S. Virani, N. D. Wong, D. Woo and M. B. Turner, *Circulation*, 2012, **125**, e2–e220.
- 16 T. C. Walther and R. V. Farese Jr., *Annu. Rev. Biochem.*, 2012, **81**, 687–714.
- 17 R. L. Reddick, S. H. Zhang and N. Maeda, *Arterioscler., Thromb., Vasc. Biol.*, 1994, **14**, 141–147.
- 18 S. Steffens, N. R. Veillard, C. Arnaud, G. Pelli, F. Burger, C. Staub, M. Karsak, A. Zimmer, J.-L. Frossard and F. Mach, *Nature*, 2005, **434**, 782–786.
- 19 L. L. Listenberger and D. A. Brown, *Curr. Protoc. Cell Biol.*, 2007, **24**, 24.2.1–24.2.11.

- 20 T. Yamane, K. Hanaoka, Y. Muramatsu, K. Tamura, Y. Adachi, Y. Miyashita, Y. Hirata and T. Nagano, *Bioconjugate Chem.*, 2011, **22**, 2227–2236.
- 21 A. Loudet and K. Burgess, *Chem. Rev.*, 2007, **107**, 4891–4932.
- 22 L. E. Jennings and N. J. Long, *Chem. Commun.*, 2009, 3511–3524.
- 23 A. Louie, *Chem. Rev.*, 2010, **110**, 3146–3195.
- 24 M. Shiomi and T. Ito, *Atherosclerosis*, 2009, **207**, 1–7.
- 25 Z. Zhang, M. T. Greenfield, M. Spiller, T. J. McMurry, R. B. Lauffer and P. Caravan, *Angew. Chem., Int. Ed.*, 2005, **44**, 6766–6769.
- 26 K. Hanaoka, K. Kikuchi, T. Terai, T. Komatsu and T. Nagano, *Chem. – Eur. J.*, 2008, **14**, 987–995.
- 27 G. Liang, J. Ronald, Y. Chen, D. Ye, P. Pandit, M. L. Ma, B. Rutt and J. Rao, *Angew. Chem., Int. Ed.*, 2011, **50**, 6283–6286.
- 28 G. S. Getz and C. A. Reardon, *Arterioscler., Thromb., Vasc. Biol.*, 2012, **32**, 1104–1115.
- 29 A. C. Doran, N. Meller and C. A. McNamara, *Arterioscler., Thromb., Vasc. Biol.*, 2008, **28**, 812–819.
- 30 H.-J. Weinmann, G. Schuhmann-Giampieri, H. Schmitt-Willich, H. Vogler, T. Frenzel and H. Gries, *Magn. Reson. Med.*, 1991, **22**, 233–237.
- 31 H.-J. Weinmann, W. Ebert, B. Misselwitz and H. Schmitt-Willich, *Eur. J. Radiol.*, 2003, **46**, 33–44.
- 32 S. Ishibashi, J. L. Goldstein, M. S. Brown, J. Herz and D. K. Bums, *J. Clin. Invest.*, 1994, **93**, 1885–1893.
- 33 J. Sanz and Z. A. Fayad, *Nature*, 2008, **451**, 953–957.
- 34 M. R. Makowski, A. J. Wiethoff, U. Blume, F. Cuello, A. Warley, C. H. P. Jansen, E. Nagel, R. Razavi, D. C. Onthank, R. R. Cesati, M. S. Marber, T. Schaeffter, A. Smith, S. P. Robinson and R. M. Botnar, *Nat. Med.*, 2011, **17**, 383–388.
- 35 S. Yasuda, K. Ikuta, T. Uwatoku, K. Oi, K. Abe, F. Hyodo, K. Yoshimitsu, K. Sugimura, H. Utsumi, Y. Katayama and H. Shimokawa, *J. Vasc. Res.*, 2008, **45**, 123–128.
- 36 M. Nahrendorf, F. A. Jaffer, K. A. Kelly, D. E. Sosnovik, E. Aikawa, P. Libby and R. Weissleder, *Circulation*, 2006, **114**, 1504–1511.
- 37 C. Burtea, S. Laurent, O. Murariu, D. Rattat, G. Toubeau, A. Verbruggen, D. Vanstherthem, L. Vander Elst and R. N. Muller, *Cardiovasc. Res.*, 2008, **78**, 148–157.
- 38 F. Chaubet, I. Bertholon, J.-M. Serfaty, R. Bazeli, H. Alsaïd, M. Jandrot-Perrus, C. Zahir, P. Even, L. Bachelet, Z. Touat, E. Lancelot, C. Corot, E. Canet-Soulas and D. Letourneur, *Contrast Media Mol. Imaging*, 2007, **2**, 178–188.
- 39 H. Alsaïd, G. De Souza, M.-C. Bourdillon, F. Chaubet, A. Sulaiman, C. Desbleds-Mansard, L. Chaabane, C. Zahir, E. Lancelot, O. Rousseaux, C. Corot, P. Douek, A. Briguet, D. Letourneur and E. Canet-Soulas, *Investig. Radiol.*, 2009, **44**, 151–158.
- 40 M. J. Lipinski, V. Amirbekian, J. C. Frias, J. G. S. Aguinaldo, V. Mani, K. C. Briley-Saebo, V. Fuster, J. T. Fallon, E. A. Fisher and Z. A. Fayad, *Magn. Reson. Med.*, 2006, **56**, 601–610.
- 41 M. Sirol, V. Fuster, J. J. Badimon, J. T. Fallon, P. R. Moreno, J.-F. Toussaint and Z. A. Fayad, *Circulation*, 2005, **112**, 1594–1600.
- 42 K. Overoye-Chan, S. Koerner, R. J. Looby, A. F. Kolodziej, S. G. Zech, Q. Deng, J. M. Chasse, T. J. McMurry and P. Caravan, *J. Am. Chem. Soc.*, 2008, **130**, 6025–6039.
- 43 A. Maiseyeu, G. Mihai, T. Kampfrath, O. P. Simonetti, C. K. Sen, S. Roy, S. Rajagopalan and S. Parthasarathy, *J. Lipid Res.*, 2009, **50**, 2157–2163.
- 44 P. M. Winter, A. M. Morawski, S. D. Caruthers, R. W. Fuhrhop, H. Zhang, T. A. Williams, J. S. Allen, E. K. Lacy, J. D. Robertson, G. M. Lanza and S. A. Wickline, *Circulation*, 2003, **108**, 2270–2274.
- 45 V. Amirbekian, M. J. Lipinski, K. C. Briley-Saebo, S. Amirbekian, J. G. S. Aguinaldo, D. B. Weinreb, E. Vucic, J. C. Frias, F. Hyafil, V. Mani, E. A. Fisher and Z. A. Fayad, *Proc. Natl. Acad. Sci. U. S. A.*, 2007, **104**, 961–966.
- 46 P. Caravan, *Acc. Chem. Res.*, 2009, **42**, 851–862.
- 47 S. Aime, M. Botta, M. Fasano and E. Terreno, *Chem. Soc. Rev.*, 1998, **27**, 19–29.
- 48 A. K. Gupta and M. Gupta, *Biomaterials*, 2005, **26**, 3995–4021.
- 49 L. Daftari Besheli, S. Aran, K. Shaqdan, J. Kay and H. Abujudeh, *Clin. Radiol.*, 2014, **69**, 661–668.
- 50 A. L. Harris, *Nat. Rev. Cancer*, 2002, **2**, 38–47.
- 51 J. M. Brown and W. R. Wilson, *Nat. Rev. Cancer*, 2004, **4**, 437–447.
- 52 P. Montcourrier, P. H. Mangeat, C. Valembois, G. Salazar, A. Sahuquet, C. Duperray and H. Rochefort, *J. Cell Sci.*, 1994, **107**, 2381–2391.
- 53 H. Izumi, T. Torigoe, H. Ishiguchi, H. Uramoto, Y. Yoshida, M. Tanabe, T. Ise, T. Murakami, T. Yoshida, M. Nomoto and K. Kohno, *Cancer Treat. Rev.*, 2003, **29**, 541–549.
- 54 T. Tsukada, M. Rosenfeld, R. Ross and A. M. Gown, *Arteriosclerosis*, 1986, **6**, 601–613.
- 55 M. Shiomi, S. Yamada and T. Ito, *Atherosclerosis*, 2005, **178**, 287–294.